

Constraints on shallow mantle viscosity from morphology and deformation of fast-spreading ridges

E. Choi¹ and W. R. Buck¹

Received 22 April 2010; revised 18 June 2010; accepted 28 June 2010; published 18 August 2010.

[1] We show that the morphology and the deformation of a fast spreading ridge constrain shallow upper mantle viscosity. A fast spreading center is simulated in a numerical model that couples tectonic deformation due to plate spreading and periodic dike emplacements. The amount of magma intruded into dikes or extruded is enough to make a 7 km thick crust and the axial lithosphere is fixed at ~2 km thickness. For low viscosities ($\leq 10^{19}$ Pa·s), the model spreading center is marked by an axial high with relief governed by the axial density structure. For high viscosities ($\geq 10^{20}$ Pa·s) the axial morphology is a valley and extensional brittle deformation is distributed away from the near-axis region. The observed morphology and deformation of fast spreading ridges are not consistent with the high mantle viscosity estimated for very dry olivine, as some suggest may result from partial melting related dehydration. **Citation:** Choi, E., and W. R. Buck (2010), Constraints on shallow mantle viscosity from morphology and deformation of fast-spreading ridges, *Geophys. Res. Lett.*, 37, L16302, doi:10.1029/2010GL043681.

1. Introduction

[2] The presence of partial melt is one of the key features that occur in the mid-ocean ridge system and plays an important role in determining the rheology of the crust and mantle in these systems. Partial melting, often facilitated by hydration, can reduce viscosity of olivine by several orders of magnitude [e.g., *Chopra and Paterson*, 1984; *Karato*, 1986]. However, experiments show that olivine's creep strength can increase by several orders of magnitude if partial melting results in dehydration due to the much higher solubility of water in the melt than in olivine [*Hirth and Kohlstedt*, 1996]. Melt rising from the source region would thus take almost all water with it leaving the residual solid olivine dry and strong. Since the potential strengthening effect of dehydration was found, researchers have been actively examining its geodynamic implications. For instance, dehydration strengthening may affect the buoyancy force of the ridge-centered plume [*Ito et al.*, 1999], the self-organized segmentation of melt upwelling at divergent boundaries [*Choblet and Parmentier*, 2001] and the development of volcanic rifted margins [*Nielsen and Hopper*, 2004; *Simon et al.*, 2009].

[3] Mantle strengthening due to melting-induced dehydration, however, has not been studied in terms of its implications on the morphology of mid-ocean ridges and the distribution of deformation around them. These observables are not only interrelated but also should be sensitive to mantle

viscosity. Which of the two competing mechanisms, i.e., dehydration strengthening or partial melt weakening, dominates below a spreading center is not clear, thus it is useful to look at the viscosity dependence of results from numerical models of spreading.

[4] Magmatic accretion at spreading centers occurs in the form of dike, sill, and extrusive emplacement. The subsequent cooling of magma generates negative buoyancy and the axial highs at fast spreading ridges can be explained as flexural response to this load [*Buck*, 2001; *Shah and Buck*, 2001]. Axial valleys, in contrast, are created when dike openings do not fully accommodate plate motions and as a result lithosphere is stretched [*Tapponnier and Francheteau*, 1978; *Chen and Morgan*, 1990a, 1990b]. These contrasting styles of accretion were once attributed to different senses of moments developing in thickening oceanic lithosphere due to non-uniform stress distributions with depth [*Phipps Morgan et al.*, 1987; *Eberle and Forsyth*, 1998; *Eberle et al.*, 1998]. More recent mid-ocean ridge models have started to explicitly consider diking in either a parameterized form [*Poliakov and Buck*, 1998; *Buck et al.*, 2005; *Ito and Behn*, 2008] or through mechanical coupling [*Qin and Buck*, 2008; *Qin*, 2008], since diking at spreading centers is also related to how lithosphere deforms [*Buck et al.*, 2005]. For instance, if dike opening accommodates all of the divergent plate motion, the lithosphere would experience negligible distributed deformation. In contrast, if dike opening accommodates only a fraction of the total spreading, significant deformation would occur within lithosphere. Dike formation itself is influenced by the stress state in the crust and mantle, which is in turn greatly influenced by mantle viscosity.

[5] In this study, we use a numerical model that mechanically couples plate motion-induced deformation with periodic dike emplacements to study the relation between mantle viscosity, axial morphology and lithospheric deformation. These relations can be used to constrain the mantle viscosity below fast spreading ridges.

2. Model Setup

[6] The model has a two-layer structure composed of crust and mantle. An elasto-visco-plastic (EVP) rheological model is assumed for both layers [e.g., *Lavier and Buck* 2002]. The 7 km-thick crust is represented by a diabase layer for which viscous behavior is assumed to follow a power law [*Mackwell et al.*, 1998], while the mantle viscosity is assumed to be constant. The elastic-brittle behavior is treated as Mohr-Coulomb plasticity without strain weakening. The two Lamé constants are 30 GPa, the friction and dilation angle is 30° and 0°, respectively, and the cohesion is 20 MPa. The mantle viscosity is changed by an order of magnitude, from 10^{18} to 10^{21} Pa·s. The density of crust and mantle is 2900 kg/m³ and

¹Lamont-Doherty Earth Observatory, Earth Institute at Columbia University, Palisades, New York, USA.

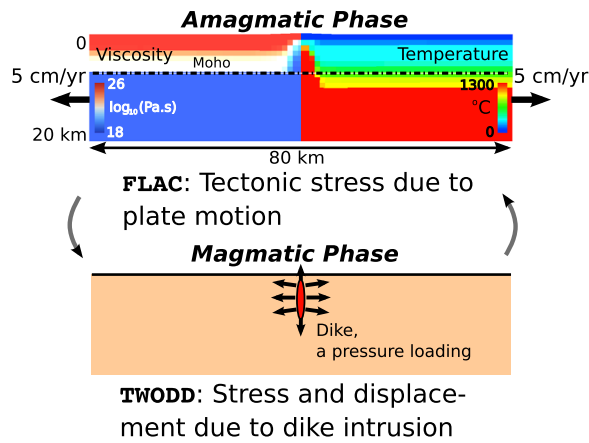


Figure 1. Schematic diagram describing the mechanical coupling of tectonic deformation due to plate motion during *amagmatic phase* and the contributions from dike emplacement during *magmatic phase*. See text for more explanations.

3300 kg/m³, respectively. Densification with cooling is not considered. The computational domain has a width of 80 km and a depth of 20 km (Figure 1). It is discretized into a regular and uniform grid with a 1 km resolution.

[7] Thermal structures are set up to have the warmest temperatures and so thinnest lithosphere at the center of the domain (Figure 1). The off-axis lithospheric thickness is 7–9 km, depending on the assumed mantle viscosity. However, a Gaussian thermal perturbation is added such that the lithospheric thickness over a low-strength zone at the spreading center is about 2 km. The top and bottom surface temperatures are 0 and 1300°C. For simplicity, advection and diffusion of heat are not considered so that the initial thermal structure remains unchanged with time, simulating a ridge system in steady-state.

3. Modeling Dike Injection

[8] We follow *Qin and Buck* [2008] and *Qin* [2008] to couple tectonic deformation due to plate motion with dike emplacement. As schematically shown in Figure 1, an *amagmatic phase* is a diking-free period. During this phase, the two sides of the domain are pulled at a constant velocity of 5 cm/yr and the bottom surface is supported by a frictionless fluid (Winkler foundation). An explicit energy-based finite difference method called FLAC is used as a numerical procedure to solve the equation of motion [e.g., *Cundall*, 1989; *Poliakov and Herrmann*, 1994; *Poliakov and Buck*, 1998].

[9] A *magmatic phase* refers to an event of dike emplacement. Since a magma injection is instantaneous compared to tectonic time scale, each diking event is considered to be a distributed pressure load acting on a vertical surface at the spreading axis. The instantaneous elastic response of a half-space to this load is computed with TWODD, a boundary element method (BEM) code [*Crouch and Starfield*, 1983]. The displacements and stresses found during a magmatic phase are added to those stored at the end of a previous amagmatic phase.

[10] The magnitude of the pressure load is defined as the difference between the tectonic stress at the end of the previous amagmatic phase and the internal pressure within dike.

The distribution of internal pressure (p_m) is given as magma's hydrostatic pressure adjusted by excess pressure:

$$p_m(z) = \rho_m g(z_t + z_m - z), \quad (1)$$

where ρ_m is magma density (2750 kg/m³), g is the gravitational acceleration, z is the depth coordinate (positive upward) with respect to the reference coordinate system, z_t is the depth to the top of dike, and z_m is a parameter that controls the excess pressure. The initial top surface of the domain is flat and at $z = 0$ level. If excess pressure is positive, an unconstrained magma column will reach a shallower level than z_t . Therefore, z_m is conceptualized as the potential height of the top of magma column relative to z_t and is called magma top. For instance, z_m of 200 m means that internal pressure can push magma up to 200 m above the dike top. z_0 is the upper bound for z_m and thus the possible maximum of excess pressure amounts to $\rho_m g z_0$. In this study z_0 is set to be 400 m. For magma pressure to be computed for only magma-filled portions of a dike, the depth coordinate, z , is bounded by $\min(z_t, z_t + z_m)$ and z_b , with z_b denoting the depth to the bottom of dike.

[11] For a given magmatic event we vary z_m and find the positions of the top and bottom of the dike where the dike opening, given by elastic displacement due to the magma pressure, becomes zero. The dike top cannot be above the surface of the crust. The actual value of z_m is iteratively varied until the dike volume computed by the BEM code becomes equal to a value called *available volume* (V_a). V_a is proportional to the drop in pressure of the magma ($=\rho_m g(z_0 - z_m)$) and is defined as

$$V_a = V_{\max}(1 - \exp[-(z_0 - z_m)/h]), \quad (2)$$

where V_{\max} is the kinematic maximum volume given by (full spreading rate) \times (diking interval) \times (lithospheric thickness) and h is an e -folding length scale. h is set to be $0.1z_0$ to ensure that V_{\max} can be reached within the ranges of typical z_m values. Since the lithosphere is close to 10 km thick off axis and the diking interval is 10 yrs in our model, V_{\max} is set to be 10^4 m². We choose the full thickness of lithosphere rather than the smallest at the spreading center because significant pressure drop can occur as deep as at the bottom of lithosphere for the given geometry of low-strength zone. Equation (2) means that tall dikes with large volume will have a low z_m , i.e., low internal pressure. This relation between internal pressure and volume in a dike may reflect a finite magma production rate. For more details such as typical depth-distributions of dike opening, we refer readers to *Qin and Buck* [2008] and *Qin* [2008].

4. Results

[12] After about 40 kyrs of model time, an axial high develops in the model with mantle viscosity of 10^{18} Pa.s (Figure 2a). The overall topography shows the combined effects of a central high built up by extruded magma and flexural response of lithosphere, as described in a previous study by *Buck* [2001]. Plastic strain is seen only in the shallow, near-axis area showing that the lithosphere experiences little internal deformation in this weak-mantle model. In contrast, for mantle with a viscosity of 10^{21} Pa.s, a 1400 m-deep rift valley develops in the model (Figure 2b) and the

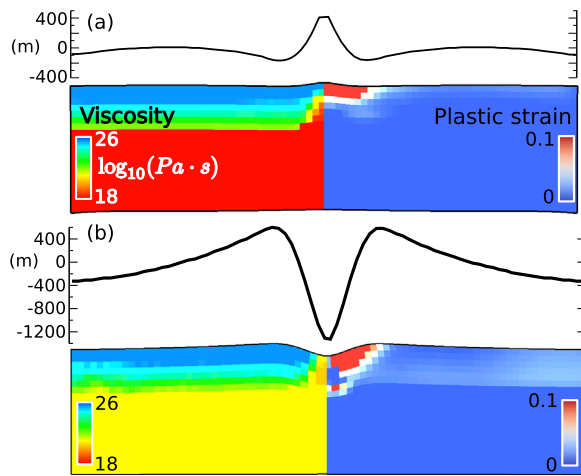


Figure 2. Model results for mantle viscosity of (a) 10^{18} Pa·s and (b) 10^{21} Pa·s. Each plot has a profile of surface topography on top and the deformed computational domain on bottom. Due to symmetry, the domain images are bisected to show viscosity field on the left half and plastic strain distribution on the right half.

plastic strain distribution is pervasive, indicating that significant deformation occurs not only at the axis but also far off-axis.

[13] Profiles of topography for various mantle viscosities are shown in Figure 3a. As mantle viscosity is changed from 10^{18} to 10^{21} Pa·s, a transition in the type of topography, from a 400 m-tall axial high to a 1400 m-deep rift valley, occurs. In accordance with the changes seen in topography, the axial height for low mantle viscosities decreases as mantle viscosity increases. Axial height reverses sign between 10^{19} to 10^{20} Pa·s (Figure 3b). Other indicators of changes induced by increased mantle viscosity include the averaged height and excess pressure of dikes. The former is given by $z_t - z_b$ and the latter is represented by magma top, z_m (Figure 3c). For the weakest mantle, dikes are about 8 km tall, always reach near the top surface, and have a near-zero steady state value of magma top (z_m). These quantities exhibit overall changes in which dike heights increase and the magma top decreases as the mantle gets stronger. In the strongest mantle case, almost all the dike events are intrusions. With height almost equal to the thickness of the domain (20 km), these intrusive dikes have considerably lower internal pressure ($z_m \cong -2$ km) and therefore cannot sustain sufficiently large openings for fully accommodating plate motion.

5. Discussion and Conclusions

[14] Our models indicate that magma has to reach a shallow level to produce axial high. Deformation of high viscosity (strong) mantle results in dynamic lowering of pressure that may limit the height to which magma can rise. This flow-related pressure reduction should be greatest where plate spreading rates are the greatest, producing axial valleys for high mantle viscosity values. However, this pressure reduction is insignificant when mantle is weak ($\leq 10^{19}$ Pa·s) and as a result, axial highs can be created. Since it is at fast spreading ridges that axial highs form, our models suggest that very little mantle strengthening occurs due to dehydration during the production of partial melt.

[15] The dynamically determined level of magma distinguishes our model from a previous model for axial high where stress-free dikes extended only down to the fixed-depth axial magma chamber [Eberle and Forsyth, 1998]. Another key assumption in our model is that the amount of magma available to open a dike is limited. The models with high viscosity mantle result in significant amount of magma being retained in the mantle during a dike event. This magma may not freeze and may even migrate to shallower depths between dike events. However, this should not alter our results since it is the height of magma intrusion and accretion during a dike event that determines the axial height. Even when assuming the lower crust at the axis has a very low viscosity, the dikes are pulled down into the high viscosity mantle.

[16] One could argue that magma pulled deep into strong mantle during a dike event might somehow migrate to shallower levels, perhaps as stresses relax in the mantle. Thus, we ran several cases with the base of the dikes fixed at 7 km depth so no magma would be pulled into the mantle. Figure 3a includes a resultant topography at 60 kyrs for one such model with a mantle viscosity of 10^{21} Pa·s. The morphology exhibits mixed characteristics of low and high mantle viscosity models. The axial height is about 150 m, a value lower than that of lower mantle viscosity models. However, the flanks have been uplifted to about 300 m by the time step shown as in other high mantle viscosity models. Therefore, a valley is still formed at the axis over the region of plate separation. Also, this model shows significant ($>10\%$) strain off-axis which is on the high side of estimated extensional strain flanking axial highs.

[17] It is often assumed that dehydration greatly increases the creep strength of dry olivine. However, our results show that if the sub-axis viscosity is so high that dynamic pressure lowering would draw melt to a spreading axis, as suggested by several authors [e.g., Spiegelman and McKenzie, 1987;

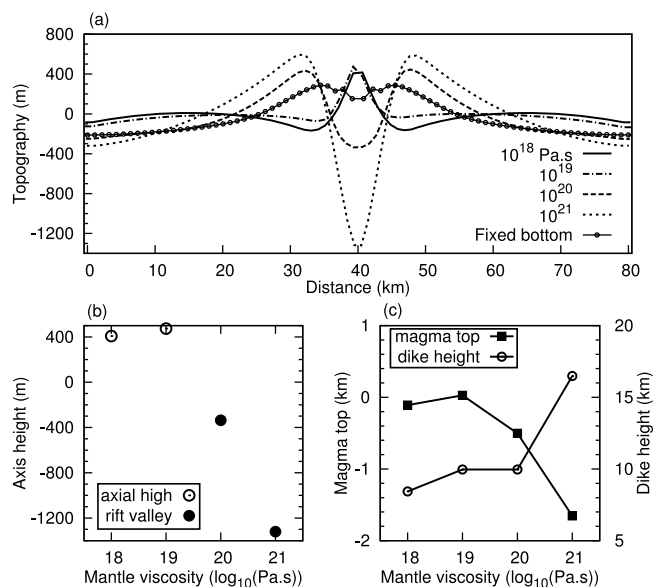


Figure 3. (a) Topography for various mantle viscosities and a model with a fixed depth (7 km) to dike bottom and the mantle viscosity of 10^{21} Pa·s. (b) Variation of axis height as a function of mantle viscosity. (c) Magma top (z_m) and dike height ($z_t - z_b$) as a function of mantle viscosity. Error range in axis height and magma top is ~ 100 m.

Ribe, 1988], then an axial high could not form at a fast-spreading center. Braun *et al.* [2000] also concluded that the sub-ridge viscosity must be low based on thermo-mechanical models for mid-ocean ridges with melting effects considered. They suggested that a viscosity as low as 10^{18} Pa·s is required for the buoyancy driven upwelling of mantle and that this is achievable through grain boundary sliding even if dehydration strengthens dry mantle. Values of mantle viscosity inferred in our study are $\leq 10^{19}$ Pa·s at depths shallower than 20 km and are consistent with experiments by Hirth and Kohlstedt [2003], where the dehydration effect was considered but shown to be insignificant at such shallow depths. In fact, we ran one case with the rheologic parameters estimated by those authors and the nonlinear viscosity was low enough that axial highs could develop.

[18] The small plastic strains at the near-axis region of our weak-mantle model are due to some combination of real lithospheric “unbending” [Buck, 2001; Buck *et al.*, 2005] and numerical errors. These strains do not significantly affect the axial height. The presence of a strong mantle, on the other hand, results in a wider region of plastic strain. Also, near-axis fault strains are large enough to produce a valley.

[19] V_{\max} , lithospheric thickness, and geometry of low strength zone are some of the parameters that are potentially important in determining the axial morphology but were not extensively explored in this study. For instance, the width of axial high is about 10 km (Figure 3a) and is less than the corresponding observed values, 40 km (e.g., $9^{\circ} 50' N$ at the East Pacific Rise). Axial relief and width of axial high are larger in models with some combination of higher V_{\max} , wider partial melt zone in lower crust, and thinner lithosphere. However, increasing V_{\max} beyond our kinematically constrained value brought about the unreasonable results that even ~ 20 km-tall dikes have high enough internal pressure to extrude magma. Effects of the parameters concerning thermal and rheological structure of mid-ocean ridges such as lithospheric thickness and geometry of low strength zone need to be studied further, but it is clear that thinner off-axis lithosphere and wider partial melt zone would generate less pressure drop for a given spreading rate. In this case, dikes have higher internal pressure causing enhanced extrusion which builds a wider axial high with larger relief.

[20] **Acknowledgments.** This work was supported by U. S. National Science Foundation grant EAR-0911565. We thank Susan Carbotte and Scott Nooner as well as two anonymous reviewers for their helpful comments.

References

- Braun, M., G. Hirth, and E. Parmentier (2000), The effects of deep damp melting on mantle flow and melt generation beneath mid-ocean ridges, *Earth Planet. Sci. Lett.*, *176*, 339–356.
- Buck, W. R. (2001), Accretional curvature of lithosphere at magmatic spreading centers and the flexural support of axial highs, *J. Geophys. Res.*, *106*, 3593–3960.
- Buck, W. R., L. L. Lavier, and A. N. B. Poliakov (2005), Modes of faulting at mid-ocean ridges, *Nature*, *434*, 719–723.
- Chen, Y., and W. J. Morgan (1990a), Rift valley/no rift valley transition at mid-ocean ridges, *J. Geophys. Res.*, *95*, 17,571–17,581.
- Chen, Y., and W. J. Morgan (1990b), A nonlinear rheology model for mid-ocean ridge axis topography, *J. Geophys. Res.*, *95*, 17,583–17,604.
- Choblet, G., and E. Parmentier (2001), Mantle upwelling and melting beneath slow spreading centers: Effects of variable rheology and melt productivity, *Earth Planet. Sci. Lett.*, *184*, 589–604.
- Chopra, P., and M. Paterson (1984), The role of water in the deformation of dunite, *J. Geophys. Res.*, *89*, 7861–7876.
- Crouch, S. L., and A. M. Starfield (1983), *Boundary Element Methods in Solid Mechanics*, 322 pp., George Allen and Unwin, London.
- Cundall, P. (1989), Numerical experiments on localization in frictional materials, *Arch. Appl. Math.*, *58*, 148–159.
- Eberle, M. A., and D. W. Forsyth (1998), An alternative, dynamic model of the axial topographic high at fast spreading ridges, *J. Geophys. Res.*, *103*, 12,309–12,320.
- Eberle, M. A., D. W. Forsyth, and E. M. Parmentier (1998), Constraints on a buoyant model for the formation of the axial topographic high on the East Pacific Rise, *J. Geophys. Res.*, *103*, 12,291–12,307.
- Hirth, G., and D. Kohlstedt (1996), Water in the oceanic upper mantle: Implications for rheology, melt extraction and the evolution of the lithosphere, *Earth Planet. Sci. Lett.*, *144*, 93–108.
- Hirth, G., and D. Kohlstedt (2003), Rheology of the upper mantle and mantle wedge; a view from the experimentalists, in *Inside the Subduction Factory*, *Geophys. Monogr. Ser.*, vol. 138, edited by J. M. Eiler, pp. 83–105, AGU, Washington, D. C.
- Ito, G., and M. D. Behn (2008), Magmatic and tectonic extension at mid-ocean ridges: 2. Origin of axial morphology, *Geochem. Geophys. Geosyst.*, *9*, Q09O12, doi:10.1029/2008GC001970.
- Ito, G., Y. Shen, G. Hirth, and C. Wolfe (1999), Mantle flow, melting, and dehydration of the Iceland mantle plume, *Earth Planet. Sci. Lett.*, *165*, 81–96.
- Karato, S. (1986), Does partial melting reduce the creep strength of the upper mantle?, *Nature*, *319*, 309–310.
- Lavier, L. L., and W. R. Buck (2002), Half graben versus large-offset low-angle normal fault: Importance of keeping cool during normal faulting, *J. Geophys. Res.*, *107*(B6), 2122, doi:10.1029/2001JB000513.
- Mackwell, S. J., M. E. Zimmerman, and D. L. Kohlstedt (1998), High-temperature deformation of dry diabase with application to tectonics on Venus, *J. Geophys. Res.*, *103*, 975–984.
- Nielsen, T. K., and J. R. Hopper (2004), From rift to drift: Mantle melting during continental breakup, *Geochem. Geophys. Geosyst.*, *5*, Q07003, doi:10.1029/2003GC000662.
- Phipps Morgan, J., E. M. Parmentier, and J. Lin (1987), Mechanisms for the origin of mid-ocean ridge axial topography: Implications for the thermal and mechanical structure of accreting plate boundaries, *J. Geophys. Res.*, *92*, 12,823–12,836.
- Poliakov, A., and W. R. Buck (1998), Mechanics of stretching elastic-plastic-viscous layers: Applications to slow-spreading mid-ocean ridges, in *Faulting and Magmatism at Mid-Ocean Ridges*, *Geophys. Monogr. Ser.*, vol. 106, edited by W. R. Buck *et al.*, pp. 305–324, AGU, Washington, D. C.
- Poliakov, A., and H. Herrmann (1994), Self-organized criticality of plastic shear bands in rocks, *Geophys. Res. Lett.*, *21*, 2143–2146.
- Qin, R. (2008), Mid-ocean ridge morphology and tectonics: Insights from numerical modeling of faults and dikes, Ph.D. thesis, Columbia Univ., Palisades, N. Y.
- Qin, R., and W. R. Buck (2008), Why meter-wide dikes at oceanic spreading centers?, *Earth Planet. Sci. Lett.*, *265*, 466–474, doi:10.1016/j.epsl.2007.10.044.
- Ribe, N. M. (1988), On the dynamics of mid-ocean ridges, *J. Geophys. Res.*, *93*, 429–436.
- Shah, A. K., and W. R. Buck (2006), The rise and fall of axial highs during ridge jumps, *J. Geophys. Res.*, *111*, B08101, doi:10.1029/2005JB003657.
- Simon, K., R. S. Huismans, and C. Beaumont (2009), Dynamical modeling of lithospheric extension and small-scale convection: Implications for magmatism during the formation of volcanic rifted margins, *Geophys. J. Int.*, *176*, 327–350, doi:10.1111/j.1365-246X.2008.03891.x.
- Spiegelman, M., and D. McKenzie (1987), Simple 2-D models for melt extraction at mid-ocean ridges and island arcs, *Earth Planet. Sci. Lett.*, *83*, 137–152.
- Tapponnier, P., and J. Francheteau (1978), Necking of the lithosphere and the mechanics of slowly-accreting plate boundaries, *J. Geophys. Res.*, *83*, 3955–3970.

W. R. Buck and E. Choi, Lamont-Doherty Earth Observatory, Earth Institute at Columbia University, PO Box 1000, 61 Rte. 9W, Palisades, NY 10964, USA. (buck@ldeo.columbia.edu; echoi@ldeo.columbia.edu)